

## Magnetoresistance and Hall effect in a disordered two-dimensional electron gas

B. L. Altshuler

*Leningrad Nuclear Physics Institute, Gatchina, Leningrad 688350 USSR*

D. Khmel'nitzkii and A. I. Larkin

*Landau Institute of Theoretical Physics, Moscow, USSR*

P. A. Lee

*Bell Laboratories, Murray Hill, New Jersey 07974*

(Received 16 April 1980)

Two models of disorder in two dimensions are discussed. The first is a localization theory that treats noninteracting particles by perturbation theory in the weak scattering limit. A weak magnetic field is found to have strong effects on the previously predicted logarithmic rise in resistivity at low temperatures. No logarithmic divergence is found for the Hall constant. A second model treats the disorder scattering by conventional diagrammatic technique but includes the effects of interactions. In a short communication it has previously been reported that the resistivity and Hall constant both show a logarithmic increase at low temperatures. The details of the calculation are reported here, together with an extension to thin wires which shows a  $T^{-1/2}$  divergence in the resistivity.

### I. INTRODUCTION

In the last year there have been a number of interesting contributions towards our understanding of electronic localization in disordered systems.<sup>1-3</sup> It has been proposed<sup>1</sup> that there exists a one-parameter scaling theory for the localization problem and that the appropriate scaling parameter is  $g(L)$ , a dimensionless number defined as the conductance in units of  $e^2/\hbar$  of a sample of size  $L$ . If such a scaling theory exists, the behavior of the conductance as a function of  $L$  is determined by the following scaling equation:

$$\frac{\partial \ln g}{\partial \ln L} = \beta(g) \quad (1.1)$$

Special interests have been focused on two dimensions, where Abrahams *et al.* argued that  $\beta \rightarrow 0$  for large  $g$ . Furthermore they proposed that  $\beta$  is a smooth monotonic function, so that it has an expansion for large  $g$  of the form

$$\beta(g) = -\frac{a}{g} + \frac{b}{g^2} \quad (1.2)$$

Equations (1.1) and (1.2) have the physical consequence that all states are localized in two dimensions, no matter how weak the disorder. The localization is logarithmic at first, changing over to exponential on a longer length scale. Equation (1.2) is supported by a perturbation theory<sup>1,3</sup> based on the summation of a certain class of diagrams which reveals contributions to the conductivity of the form  $-(2\pi^2)^{-1} \ln L$ . Thus the perturbation theory is consistent with

$a = (2\pi^2)^{-1}$ . This consistency is checked to second order with the demonstration<sup>3</sup> that conductivity diagrams of order  $g^{-1}(\ln L)^2$  sum to zero. The coefficient  $b$  has recently been shown to vanish<sup>4</sup> by summing terms of order  $g^{-1} \ln L$ . These results are in agreement with those obtained by Wegner<sup>2</sup> using a quite different approach.

We should mention two pieces of work that are in disagreement with the above references. Using the memory-functional approach, Götze and co-workers<sup>5</sup> obtained a result different from the above in that  $a = 0$  and  $b$  is finite. We comment that Götze did not consider the class of diagrams included in Refs. 1 and 3, so that it is not difficult to understand why he obtained  $a = 0$ . Furthermore his finite  $b$  comes from singular contributions to the conductivity of the form  $g^{-1} \ln L$  which arises from the vanishing energy denominator of the diffusion pole. A direct calculation<sup>4</sup> (rather than via the memory-functional approach) shows that all  $g^{-1} \ln L$  terms arising from the diffusion pole alone also cancel, in contrast with the  $b \neq 0$  result of Ref. 5. A second work that is in disagreement with the one-parameter scaling theory is a numerical implementation of the general scaling idea.<sup>6</sup> The numerical results are more consistent with  $\beta = 0$  for  $g$  greater than a certain critical value. However the numerical approach is an approximate one, valid for small  $g$ , and is subject to systematic error for intermediate values of  $g$ .

Commenting further on the perturbation theory, it has been found that the cancellations that led to the logarithmic singularity in the perturbation theory is

extremely delicate. For example, introduction of a random local magnetic field (to simulate magnetic impurities) is sufficient to cut off the singularity.<sup>7</sup> These calculations have also been done for spin-orbit scattering.<sup>8</sup> While spin-orbit scattering does not cut off the divergence, its effect is to produce a leading contribution to the  $\beta$  function of the opposite sign, i.e.,  $a = -(4\pi^2)^{-1}$ . Such a result implies an infinite conductivity for  $g$  greater than a certain critical value. At the very least, such a strange result means that a much deeper understanding of the structure of the perturbation theory is required.

A logarithmic rise in resistivity at low temperatures has been observed in thin films<sup>9</sup> and in the silicon inversion layer.<sup>10</sup> Many features are in agreement with predictions based on Eqs. (1.1) and (1.2). However the experimental systems all involve a Fermi sea of interacting electrons whereas the localization theory is a strictly single-particle theory. The effects of interactions on a disordered system in the metallic regime (i.e.,  $k_F l \gg 1$ , where  $l = v_F \tau$  is the electron mean-free path) must be investigated. The result<sup>11,12</sup> shows that interactions effects alone (without the effects of localization) also produce a logarithmic rise in resistivity consistent with the experimental observations.

This paper is divided into two parts. In the first part we try to develop further understanding of the perturbation theory of localization by extending the work of Refs. 1 and 3 to various physical situations. We consider the effects of a magnetic field on the logarithmic singularity in the resistivity. The Hall coefficient is then calculated. In the second part we focus on the interaction effects while ignoring localization. The Hall coefficient is calculated and contrasted with the localization theory prediction. In the course of our presentations, the conductivity calculation will also be reviewed so that details omitted in earlier brief communications will be supplied. We also present results for the resistivity in 1D that is appropriate for thin wires. The predictions for the two theories are very different and it is hoped that this work will help clarify the comparison between theory and experiments.

## II. MAGNETORESISTIVITY IN THE LOCALIZATION THEORY

We begin by reviewing the perturbation theory<sup>1,3</sup> for the conductivity at frequency  $\Omega$  that leads to the logarithmic divergence in the absence of a magnetic field. The divergence occurs in the summation of the set of maximally crossed diagrams shown in Fig. 1(a). It is instructive to show the diagram in an equivalent way shown in Fig. 1(b). The maximally crossed diagram in the particle-hole propagator becomes a ladder diagram in the particle-particle propagator

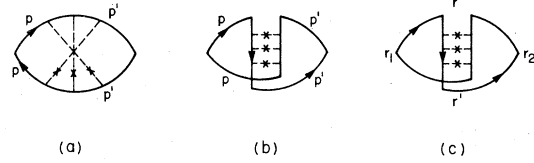


FIG. 1. (a) Lowest-order logarithmic correction to the conductivity diagram; (b) Fig. 1(a) redrawn to emphasize the ladder diagram in the particle-particle channel; and (c) the same diagram in real-space representation.

$P(\vec{p} + \vec{p}', \Omega)$  which satisfies the Dyson equation

$$P(\vec{p} + \vec{p}', \Omega) = u^2 + u^2 P_0(\vec{p} + \vec{p}', \Omega) P(\vec{p} + \vec{p}', \Omega) , \quad (2.1)$$

where  $\tau^{-1} = 2\pi N_1 u^2$  is the scattering rate,  $N_1$  is the single spin density of states, and  $u^2$  represent the mean-square impurity potential. The kernel

$$\begin{aligned} P_0(\vec{p} + \vec{p}', \Omega) &= \sum_{\vec{p}_1} G_-(p_1, \epsilon) G_+(-\vec{p}_1 + \vec{p} + \vec{p}', \epsilon + \Omega) \\ &= 2\pi N_1 \tau [1 - \tau D(\vec{p} + \vec{p}')^2 + i\Omega\tau] , \quad (2.2) \end{aligned}$$

where  $G_{\pm}(p, \omega) = [\omega - \epsilon(p) \pm i/2\tau]^{-1}$  and  $D = \frac{1}{2} v_F^2 \tau$  is the diffusion coefficient in 2D. Combining Eqs. (2.1) and (2.2), we obtain

$$P(\vec{p} + \vec{p}', \Omega) = u^2 \tau^{-1} [-i\Omega + D(\vec{p} + \vec{p}')^2]^{-1} . \quad (2.3)$$

The most direct way to see Eq. (2.3) is that if the arrow on one of the particle lines is reversed and its momentum replaced by its opposite sign, the diagram is identical to a particle-hole ladder which is well known to have a diffusion pole of the form shown in Eq. (2.3). From Eq. (2.3) it is readily seen that upon integration over  $p, p'$  to obtain the conductivity, the region of integration near  $\vec{p}' = -\vec{p}$  leads to a logarithmic term  $\ln \Omega$  in 2D

$$\delta\sigma = \frac{e^2}{\hbar} \frac{s}{4\pi^2} \ln|\Omega\tau| , \quad (2.4)$$

where  $s$  is the spin and other, such as orbital, degeneracy.

While the diffusion pole in the particle-hole propagator follows from particle conservation the same cannot be said of the particle-particle propagator. In particular if the particle-hole transformation just discussed is violated, it is possible that the pole in Eq. (2.3) may be cut off. This is what happened in the case of spin-flip scattering.<sup>7</sup> As we shall see, application of a magnetic field also introduces a cutoff.

In the presence of a magnetic field the conductivity transverse to the magnetic field should be calculated

in the coordinate representation as shown in Fig. 1(c). Impurity averaging effectively introduces a short range interaction between electrons and it suffices to study the propagator  $P(\bar{r}, \bar{r}', \Omega)$  which satisfies the Dyson equation

$$\begin{aligned} \bar{P}(\bar{r}, \bar{r}', \Omega) &= u^2 \delta(\bar{r} - \bar{r}') + u^2 \sum_{\bar{r}_1} \bar{P}_0(\bar{r}, \bar{r}_1, \Omega) \bar{P}(\bar{r}_1, \bar{r}', \Omega), \end{aligned} \quad (2.5)$$

where

$$\bar{P}_0(\bar{r}, \bar{r}_1) = \bar{G}_-(\bar{r}, \bar{r}_1, \epsilon) \bar{G}_+(\bar{r}, \bar{r}_1, \epsilon + \Omega) \quad (2.6)$$

$$\bar{P}_0(\bar{r}, \bar{r}', \Omega) = 2\pi N_{1\tau} \sum_{n,\alpha} \psi_{n,\alpha}(\bar{r}') \psi_{n,\alpha}^*(\bar{r}) \left[ 1 - 4\tau D \left( \frac{eH}{\hbar c} \right) \left( n + \frac{1}{2} \right) + i\Omega\tau \right], \quad (2.8)$$

where  $\psi_{n,\alpha}$  denotes the set of Landau orbits for a doubly charged particle. Combining Eqs. (2.5) and (2.8) we obtain

$$\bar{P}(\bar{r}, \bar{r}', \Omega) = \frac{u^2}{\tau} \sum_{n,\alpha} \frac{\psi_{n,\alpha}(\bar{r}) \psi_{n,\alpha}^*(\bar{r}')}{4D(eH/\hbar c)(n + \frac{1}{2}) - i\Omega} \quad (2.9)$$

The conductivity can now be calculated by combining Eq. (2.9) with

$$\begin{aligned} \bar{G}_+(\bar{r}_1, \bar{r}, \epsilon + \Omega) \bar{G}_+(\bar{r}', \bar{r}_2, \epsilon + \Omega) \\ \times \bar{G}_-(\bar{r}_2, \bar{r}, \epsilon) \bar{G}_-(\bar{r}', \bar{r}_1, \epsilon) \end{aligned}$$

Noting that  $G$  has a range in space given by the mean-free path  $l$ , the important region of integration is for  $|\bar{r} - \bar{r}'| \approx l$ . On the other hand the  $n$ th term in the sum in Eq. (2.9) is slowly varying on a length scale small compared with the cyclotron radius of the  $n$ th Landau orbit. We can then limit the sum to  $n < n_m$  where  $n_m = (\hbar c/2eH)l^{-2}$  and set  $\bar{r} = \bar{r}'$ . The integration over the four  $G$ 's is the same as in the absence of a magnetic field. Upon integrating  $\bar{P}(\bar{r}, \bar{r})$  over  $\bar{r}$ , we obtain

$$\begin{aligned} \delta\sigma_H(\Omega) &= -\frac{s}{4\pi^2} \frac{e^2}{\hbar c} \frac{4H}{\hbar c} \sum_{n=0}^{n_m} \text{Re} \left[ 4 \frac{DeH}{\hbar c} \left( n + \frac{1}{2} \right) - i\Omega \right]^{-1} \end{aligned} \quad (2.10)$$

The magnetic field of interest is usually sufficiently small so that  $n_m \gg 1$  in which case Eq. (2.10) becomes

$$\delta\sigma_H = \frac{s}{(2\pi)^2} \frac{e^2}{\hbar c} \left[ \psi \left( \frac{1}{2} - \frac{i\Omega}{D} \left( \frac{\hbar c}{4eH} \right) \right) + \ln \left[ 4 \frac{eH}{\hbar c} D\tau \right] \right], \quad (2.11)$$

and  $\bar{G}$  is the Green's function in a magnetic field. If the Landau orbit is much larger than the Fermi wavelength, we can use the quasiclassical approximation<sup>13</sup>

$$\bar{G}(\bar{r}, \bar{r}') = \exp \left[ ie \int_{\bar{r}}^{\bar{r}'} \bar{A}(\bar{T}) \cdot d\bar{T} \right] G(\bar{r} - \bar{r}'), \quad (2.7)$$

where the integral is along a straight line connecting  $\bar{r}$  and  $\bar{r}'$ . The quantity  $\bar{P}_0$  is well known in the theory of dirty superconductors. Its calculation is shown in Appendix A for completeness, and we obtain

where  $\psi$  is the digamma function. If  $\Omega(\hbar c/4eH)/D \gg 1$ ,  $\psi$  approaches a logarithm, and we recover the  $\ln \Omega\tau$  divergence in Eq. (2.4). In the opposite limit, the second term in Eq. (2.11) dominates and a logarithmic dependence on  $H$  is predicted. The sensitivity to a magnetic field is a consequence of the peculiar structure of the maximally crossed diagram (Fig. 1); the particle and hole move along opposite paths in space so that the phase factors in Eq. (2.7) add instead of cancel.

Let us now adopt the interpretation<sup>14,15</sup> that at finite temperatures  $\Omega$  is to be replaced by the inelastic scattering rate  $\tau_m^{-1}$ . Equation (2.11) then yields a critical  $H_c$  given by

$$4eH_c/\hbar c = (D\tau_{in})^{-1}. \quad (2.12)$$

Equation (2.12) states that the size of the lowest Landau orbital is comparable to the diffusion length in the time  $\tau_{in}$ . Note that  $H_c$  can be extremely small. For instance, a diffusion length of  $10^{-4}$  cm corresponds to  $H_c = 10$  G.

### III. HALL EFFECT IN THE LOCALIZATION THEORY

The Hall current is the current response that is linear in an electric field and a magnetic field. Let us define  $i\Omega \bar{A}_1 = \bar{E}$  and  $i\bar{k} \times \bar{A}_2 = \bar{H}$ . The kinetic energy is of the form

$$\begin{aligned} H &= \frac{1}{2m} [\bar{p} + e(\bar{A}_1 + \bar{A}_2)]^2 \\ &= \frac{p^2}{2m} + \frac{e}{m} \bar{p} \cdot (\bar{A}_1 + \bar{A}_2) + \frac{e^2}{2m} (\bar{A}_1 + \bar{A}_2)^2. \end{aligned} \quad (3.1)$$

The Hall current is proportional to  $\vec{E} \times \vec{H}$  which can be written as  $\Omega [\vec{A}_2(\vec{k} \cdot \vec{A}_1) - \vec{k}(\vec{A}_1 \cdot \vec{A}_2)]$ . We note that the term  $\vec{A}_2(\vec{k} \cdot \vec{A}_1)$  can be obtained from a second-order perturbation theory in the second term in Eq. (3.1) whereas the term  $\vec{k}(\vec{A}_1 \cdot \vec{A}_2)$  also has contributions from a first-order perturbation in the last term in Eq. (3.1). Thus it is simpler to look for the former term.

$$\vec{j}_a = \frac{ie^3}{m^3} \int_0^\Omega \frac{d\epsilon}{2\pi} \sum_{\vec{p}} G_+(\vec{p}) G_+(\vec{p} + \vec{k}) G_-(\vec{p}) (\vec{A}_1 \cdot \vec{p}) (\vec{A}_2 \cdot \vec{p}) (\vec{p} + \vec{k}/2) \quad (3.2)$$

We want to keep terms to first order in  $\vec{k} \cdot \vec{A}_1$ . This can come only from an expansion of  $G_+(\vec{p} + \vec{k})$  since the contribution from the last term in Eq. (3.2) will be proportional to  $(\vec{A}_1 \cdot \vec{A}_2) \vec{k}$ . Upon expansion we can do the  $\vec{p}$  integration by separating the angular and radial components

$$\vec{j}_a = \frac{i\Omega e^3}{m^4} F_1 \int \frac{p dp}{(2\pi)^2} p^4 \frac{1}{p^2/2m - \epsilon_F + i/2\tau} \frac{1}{(p^2/2m - \epsilon_F - i/2\tau)^3} \quad (3.3)$$

where

$$F_1 = \int \frac{d\theta}{2\pi} (\vec{A}_1 \cdot \hat{p}) (\vec{A}_2 \cdot \hat{p}) (\vec{k} \cdot \hat{p}) \hat{p} = \frac{1}{8} [(\vec{A}_1 \cdot \vec{k}) \vec{A}_2 + (\vec{A}_1 \cdot \vec{A}_2) \vec{k} + (\vec{A}_2 \cdot \vec{k}) \vec{A}_1] \quad (3.4)$$

Again, only the first term in Eq. (3.4) is of interest to us. The  $p$  integration in Eq. (3.3) can now be done, giving

$$\vec{j}_a = -\frac{i}{2} \frac{\Omega}{2\pi} \frac{e^3}{m} (\vec{A}_1 \cdot \vec{k}) \vec{A}_2 \tau^3 \left( \epsilon_F^2 - \frac{i\epsilon_F}{\tau} \right) \quad (3.5)$$

Note that care must be taken to evaluate the  $p^4$  term in the numerator in the integral at the pole, yielding the second term in Eq. (3.5).

Diagram 2(b) can be calculated in the same way, and we obtain  $\vec{j}_b = -\vec{j}_a^*$ . Thus we obtain the Hall current

$$j_H = \sigma_H \hat{H} \times \vec{E} \quad (3.6)$$

where  $\sigma_H = s(e^3 H/m) \epsilon_F \tau^2 / 2\pi$  in agreement with the

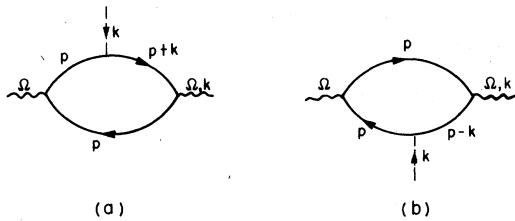


FIG. 2. Diagrams for the Hall effect. Dashed line carries momentum  $k$  and represents linear response in the magnetic field.

Our strategy is to write down the usual conductivity diagram, and then insert a magnetic field vertex which carries a momentum  $k$  into each Green's function  $G(\vec{p})$ . Each magnetic vertex is assigned a value  $e\vec{A}_2 \cdot (\vec{p} + \vec{k}/2)/m = e\vec{A}_2 \cdot \vec{p}/m$ . It is instructive to test this on the lowest-order diagram shown in Fig. 2. Figure 2(a) makes the following contribution to the current

usual transport theory ( $s$  is the spin and other degeneracies).

Now we are ready to calculate the Hall effect in the localization theory. Figures 3 are generated by inserting the magnetic vertex in every possible way into Fig. 1(a). (It is easy to show that insertion into opposite sides of the particle-particle ladder cancel each other.) We expand the  $k$  dependence in  $G(\vec{p} \pm \vec{k})$  as before. Figures 3(c) and 3(d) equals minus the complex conjugate of Figs. 3(a) and 3(b). Together we have

$$\delta \vec{j}_H = \frac{ise^3 \Omega}{2\pi m^3} P_1 P_2 \quad (3.7)$$

where

$$P_1 = \sum_{\vec{q}} P(\vec{q}, \Omega) = \frac{-u^2 \ln \Omega \tau}{4\pi D \tau} \quad (3.8)$$

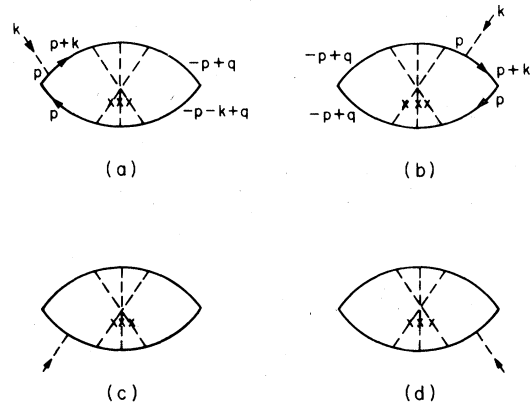


FIG. 3. Diagrams for the Hall effect obtained by inserting the magnetic vertex (dashed line carrying momentum  $k$ ) in Fig. 1(a).

is from the particle-particle ladder as in the conductivity calculation, and

$$P_2 = \frac{1}{m} \sum_{\vec{p}} 2[G_+^4(\vec{p})G_-^2(\vec{p}) - \text{c.c.}] \times (\vec{A}_1 \cdot \vec{p})(\vec{A}_2 \cdot \vec{p})(\vec{k} \cdot \vec{p})(-\vec{p})$$

$$= -i4m^2\epsilon_F\tau^4(\vec{A}_1 \cdot \vec{k})\vec{A}_2. \quad (3.9)$$

Here the angular and radial  $\vec{p}$  integration is evaluated as in Eq. (3.5). The result is that

$$\delta j_H = \delta\sigma_H \hat{H} \times \vec{E}, \quad (3.10)$$

where

$$\delta\sigma_H = \frac{se^3H}{m} \frac{2\tau}{(2\pi)^2} \ln|\Omega\tau|. \quad (3.11)$$

Comparing with Eq. (3.6) we have

$$\frac{\delta\sigma_H}{\sigma_H} = \frac{2}{2\pi\epsilon_F\tau} \ln|\Omega\tau|. \quad (3.12)$$

Experimental measurements of Hall effect are usually expressed in terms of the Hall constant  $R_H = E_y/j_x H = \sigma_H/(\sigma^2 H)$ . Combining Eqs. (3.12) and (2.4) we obtain

$$\delta R_H/R_H = 0, \quad (3.13)$$

where  $R$  is the resistance per square. In the free electron model,  $R_H = (nec)^{-1}$ , so that a naive interpretation would state that the logarithmic correction is in the scattering rate, and not in the carrier density. This result for the Hall constant was first obtained by Fukuyama.<sup>16</sup>

#### IV. HALL EFFECT IN THE INTERACTING FERMION SYSTEM

In this section we purposely ignore the complications due to the crossed diagrams treated in earlier sections. We assume that such diagrams have been suppressed by any one of the mechanisms already discussed, such as magnetic field and spin-flip scattering. (This point is further discussed in Appendix B.) Instead the impurity scattering is treated by the conventional diagrammatic technique in the  $k_F l \gg 1$  limit and we include the effects of electron electron interaction to lowest order.<sup>11,12</sup> The interaction is taken to be the dynamically screened Coulomb interaction

$$v_s(q, \omega) = v_B(q)/[1 + v_B(q)\Pi(q, \omega)], \quad (4.1)$$

where  $v_B(q) = 2\pi e^2/|\vec{q}|$  is the bare interaction in 2D

and

$$\Pi(q, i\omega_n) = sN_1 Dq^2/(|\omega_n| + Dq^2). \quad (4.2)$$

Here  $N_1 = m/2\pi$  is the single spin density of states. In the small  $q, \omega$  limit, and subject to the condition  $D\kappa q \gg |\omega_n|$  where  $\kappa = e^2 s N_1$  is the screening constant

$$v_s(q, i\omega_n) = \frac{1}{sN_1} \frac{|\omega_n| + Dq^2}{Dq^2} \quad (4.3)$$

and is independent of the bare coupling  $e^2$ .

As in the last section we calculate the Hall current by inserting an additional vertex into the conductivity diagrams. The conductivity results have been reported before<sup>11,12</sup> but we take this opportunity to supply some details. The important feature is that vertex correction as shown in Fig. 4 gives rise to diffusive-like divergence for small  $q$  and  $\omega$

$$\Gamma(q, \omega_m, \epsilon_n) = \begin{cases} (|\omega_m| + Dq^2)^{-1} \tau^{-1}, & \text{if } \epsilon_n(\epsilon_n - \omega_m) < 0 \\ 1 & \text{otherwise.} \end{cases} \quad (4.4)$$

The diagrams that contribute to the conductivity are shown in Fig. 5. These diagrams are generated in a conserving approximation from an exchange self-energy diagram [Fig. 7(a)]. In Appendix C we show that the sum of diagrams (a), (b), and (c) is exactly zero so that the conductivity correction comes only from Figs. 5(d) and 5(e). In the following we present the calculation for zero temperature. The finite temperature case proceeds along similar lines and we simply give the result.

We begin by doing the momentum sum in the electron Green's function. The sum factorizes into two parts on either side of the impurity ladder. Let us label by  $\vec{M}$  the left side of Fig. 5(d). Note that in order to obtain the divergence given in Eq. (4.4), we must have  $\epsilon, \epsilon + \Omega$  positive and  $\epsilon + \Omega + \omega$  negative and vice versa. Thus we obtain

$$\vec{M}(\vec{q}) = \int \frac{d^2\vec{p}}{(2\pi)^2} G_+^2(\vec{p}) G_-(\vec{p} + \vec{q}) \frac{\vec{p}}{m}$$

$$= \int \frac{d^2\vec{p}}{(2\pi)^2} G_+^2(\vec{p}) G_-^2(\vec{p}) \left[ \vec{q} \cdot \frac{\vec{p}}{m} \right] \frac{\vec{p}}{m}$$

$$= 2\epsilon_F\tau^3 \vec{q}. \quad (4.5)$$

Next we note that the integrand for diagram (d) and

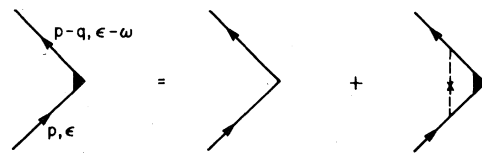


FIG. 4. Vertex correction.

(e) are the same, except that (d) is proportional to  $\bar{M}(q)\bar{M}(q)$  while (e) is proportional to  $\bar{M}(\bar{q}) \times \bar{M}(-\bar{q}) = -\bar{M}(\bar{q})\bar{M}(\bar{q})$  so (d) and (e) are opposite in sign. However, care must be taken in writing down the region of integration. For  $\epsilon > 0$ , we denote the contribution from Figs. 5(d) and 5(e) by  $d_+$  and  $e_+$ , respectively, and it turns out that the region of integration is the same so that  $d_+ + e_+ = 0$ . For

$\epsilon < 0$ , however, the conditions are

$$\epsilon + \Omega < 0, \quad \epsilon + \omega + \Omega > 0 \quad \text{for } d_-$$

and

$$\epsilon + \Omega < 0, \quad \epsilon + \omega > 0 \quad \text{for } e_- .$$

Thus the sum is

$$d_- + e_- = ise^2 \int_{-\infty}^{-\Omega} \frac{d\epsilon}{2\pi} \int_{-\epsilon-\Omega}^{-\epsilon} \frac{d\omega}{2\pi} \int \frac{d^2q}{(2\pi)^2} \int \frac{\bar{M}(\bar{M} \cdot \bar{A})u^2}{-i(\omega + \Omega) + Dq^2} \frac{iv_s(q, \omega)}{(-i\omega + Dq^2)^2\tau^3} \quad (4.6)$$

In Eq. (4.6) the first diffusion pole comes from the impurity ladder and the  $(-i\omega + Dq^2)^{-2}$  comes from the vertex correction to  $v_s$ . Equation (4.6) must be combined with the other pair of diagrams similar to Figs. 5(d) and 5(e) but with the dressing of the particle and the hole line interchanged. In this case it is the  $\epsilon < 0$  part that cancels while the  $\epsilon > 0$  part exactly equals Eq. (4.6). Thus we obtain

$$\delta \bar{j} = 2ise^2 \int_{\Omega}^{\infty} \frac{d\epsilon}{2\pi} \int_{\epsilon-\Omega}^{\epsilon} \frac{d\omega}{2\pi} \frac{\bar{M}(\bar{M} \cdot \bar{A})u^2}{-i(\omega + \Omega) + Dq^2} \frac{iv_s(q, \omega)}{(-i\omega + Dq^2)^2\tau^3} \quad (4.7)$$

We note that the expression Eq. (4.4) is valid only for  $\omega\tau \ll 1$  so that the  $\omega$  integration must be cut off. Since the integrand is independent of  $\epsilon$  we can rearrange the integration as follows:

$$\int_{\Omega}^{\infty} d\epsilon \int_{\epsilon-\Omega}^{\epsilon} d\omega = \int_0^{\infty} d\epsilon \int_{\epsilon}^{\epsilon+\Omega} d\omega = \int_0^{\Omega} d\omega \int_0^{\omega} d\epsilon + \int_{\Omega}^{\infty} d\omega \int_{\omega-\Omega}^{\omega} d\epsilon = \int_0^{\Omega} d\omega\omega + \Omega \int_{\Omega}^{\infty} d\omega \quad (4.8)$$

The second term in Eq. (4.8) is more singular in the small  $\omega$  limit and is the dominant term. Using the asymptotic form Eq. (4.3) and Eq. (4.5) into Eq. (4.7) we obtain

$$\delta \bar{j} = \frac{i\Omega}{2\pi} 2se^2 \int_{\Omega}^{1/\tau} \frac{d\omega}{2\pi} \int \frac{d^2q}{(2\pi)^2} \frac{i(2\epsilon_F\tau^3)^2 \bar{q}(\bar{q} \cdot \bar{A})u^2}{[-i(\omega + \Omega) + Dq^2](-i\omega + Dq^2)sN_1 Dq^2\tau^3} \quad (4.9)$$

The use of Eq. (4.3) is justified because the important region of  $q$  integration is  $Dq^2 \approx \omega$  due to the divergence of the integrand, so that the condition  $Dq\kappa \gg \omega$  is satisfied. We remark that this is not the case in the density of states calculation, in which case the full Eq. (4.1) must be used, leading to the  $(\ln\Omega)^2$  result given in Eq. (10) of Ref. 11. Return-

ing to Eq. (4.9), the integral is clearly logarithmically divergent, giving

$$\delta \bar{j} = i\Omega \bar{A} \delta\sigma \quad (4.10)$$

where

$$\delta\sigma = \frac{e^2}{\hbar c} \frac{1}{2\pi^2} \ln|\Omega\tau| \quad (4.11)$$

The above computation can easily be performed at finite temperature by using imaginary frequencies and analytic continuation to the real axis. Not unexpectedly the result is

$$\delta\sigma = \frac{e^2}{\hbar c} \frac{1}{2\pi^2} \ln T\tau \quad (4.12)$$

when  $T \gg \Omega$ .

In Ref. 11 we have shown that for a short-range interaction the Hartree term also becomes important. Diagrams similar to Fig. 5 can be generated and the total conductivity correction is

$$\delta\sigma = \frac{e^2}{\hbar c} \frac{1}{4\pi^2} (2 - 2F) \ln|\Omega\tau| \quad (4.13)$$

where  $F$  is given in Appendix B.

In view of the experimental interest in thin wires,<sup>17</sup>

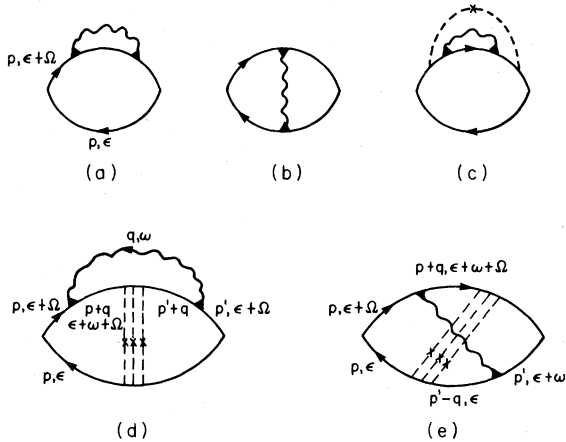


FIG. 5. Diagrams contributing to conductivity to first order in interaction (wavy line).

we digress to discuss the one-dimensional situation. In a strictly one-dimensional system, the localization length equals the mean-free path  $l$ , and the treatment here is not adequate. However in a thin wire of cross section  $d \times d$ , the localization length  $\xi$  can be much greater than  $l$ . The cutoff length scale of the present treatment is  $(D/T)^{1/2}$ . If this length is much less than  $\xi$ , the effects of localization are not yet apparent, and the present treatment is valid. Furthermore the divergent contribution in Eq. (4.9) comes from the small  $\bar{q}$  limit. If  $(D/\Omega)^{1/2}$  or  $(D/T)^{1/2}$  is much greater than  $d$  we must replace the usual

$$\frac{1}{\text{vol}} \sum_{\bar{q}} \rightarrow \frac{1}{d^2} \int \frac{dq_z}{2\pi}, \quad (4.14)$$

even though other aspects of the problem that involve short distances, such as the diffusion constant  $D$ , should remain three dimensional. The integral in Eq. (4.9) is easily done and we obtain

$$\delta\sigma_{ex} = -\frac{1}{d^2} \frac{e^2}{\hbar c} \frac{2}{\pi} \left( \frac{D}{2T} \right)^{1/2}. \quad (4.15)$$

Equation (4.15) is the exchange contribution to the conductivity. We must add the Hartree contribution just as in Eq. (4.13). We recall that in 2D the real and imaginary part of  $v_s(q, \omega)$  make equal contributions to the exchange term, whereas only the real part contribute to the Hartree correction. Putting in a factor of 2 for the spin in the Hartree term, we obtain Eq. (4.13). An interesting difference arises in the 1D case. A simple calculation shows that the imaginary part of  $v_s(q, \omega)$  contributes three times as much as the real part to the exchange term. Inclusion of the Hartree term thus gives

$$\delta\sigma = -\frac{1}{d^2} \frac{e^2}{\hbar c} \frac{1}{2\pi} \left( \frac{D}{2T} \right)^{1/2} (4 - 2F'), \quad (4.16)$$

where  $F'$  is given by Eq. (B1) but evaluated for a 3D Fermi surface.  $F'$  also approaches unity if  $2k_F/\kappa \rightarrow 0$  and zero for large  $2k_F/\kappa$ . Whereas in 2D the conductivity corrections cancels for short screening length, the divergence in 1D survives even in this limit. From Eq. (4.16) we also see that the correction to

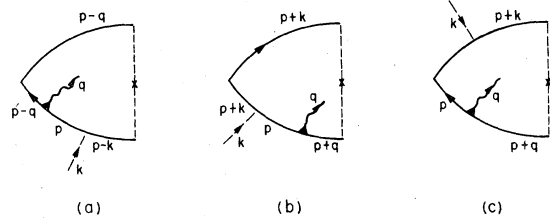


FIG. 6. Different ways of inserting a magnetic vertex (dashed line) into the  $\bar{M}$  factor [half of the conductivity diagrams shown in Figs. 5(d) and 5(e)].

the conductivity is inversely proportional to the cross-sectional area  $d^2$ . This is in agreement with experimental observation.<sup>17</sup> Again it is interesting to note that Eq. (4.16) has the same functional form as the prediction of localization theory if  $T$  is replaced by  $\tau_m^{-1}$ . Eq. (4.16) says that if  $T \gg \tau_m^{-1}$ , interactions effects will produce corrections to the conductivity on a length scale such that localization effects are not yet significant. Furthermore, unlike 2D, Eq. (4.16) predicts a quite different absolute value for the correction compared with the localization theory and could easily be tested experimentally.

It is worth pointing out that in 3D the situation is reversed, so that the real part of  $v_s(q, \omega)$  contribute three times as much as the imaginary to the exchange correction. Inclusion of the Hartree term thus gives a correction to the conductivity of the form  $T^{1/2}(4 - 6F')$ . Thus the correction can change sign depending on the screening length.

Now we are ready to compute the Hall current. As in Sec. III, we insert a magnetic vertex in all possible ways into the conductivity diagrams. Insertions into the particle-hole ladder are found to cancel, just as the case for the particle-particle ladder. In Appendix D we show that the diagrams derived from the conductivity diagrams [Figs. 5(a), 5(b), and 5(c)] also cancel each other. So we are left with diagrams derived from Figs. 5(d) and 5(e), which can be broken up into two pieces, each of which was labeled by  $\bar{M}$  earlier. We first consider the electromagnetic vertex which carries no momentum. Figure 6 shows the possible ways of inserting a magnetic vertex into  $\bar{M}$ . Recalling that  $\bar{M}$  is linear in  $\bar{q}$ , we must look for terms linear in both  $\bar{q}$  and  $\bar{k}$ , i.e., terms of the form  $(\bar{A}_2 \cdot \bar{q})\bar{k}$ . Figures 6(a), 6(b), and 6(c) have the following values:

$$\bar{M}_a = (\bar{A}_2 \cdot \bar{p})(\bar{p} - \bar{q})G_-(\bar{p} - \bar{k})G_-(\bar{p})G_+^2(\bar{p} - \bar{q}) \quad (4.17a)$$

$$= (\bar{A}_2 \cdot \bar{p})\bar{q} \left[ \bar{k} \cdot \frac{\bar{p}}{m} \right] G_+^2 G_+^2 + 2(\bar{A}_2 \cdot \bar{p})\bar{p} \left[ \bar{k} \cdot \frac{\bar{p}}{m} \right] \left[ \bar{q} \cdot \frac{\bar{p}}{m} \right] G_+^2 G_+^2. \quad (4.17b)$$

The first term in Eq. (4.17b) is proportional to  $\bar{A}_2 \cdot \bar{k}$  upon the angular  $\bar{p}$  integration and therefore vanishes.

$$\begin{aligned} \bar{M}_b &= (\bar{A}_2 \cdot \bar{p})(\bar{p} + \bar{k})G_-(p+q)G_+(\bar{p})G_+^2(\bar{p} + \bar{k}) \\ &= (\bar{A}_2 \cdot \bar{p}) \left[ \bar{k} \bar{q} \cdot \frac{\bar{p}}{m} \right] G_-^2 G_+^3 + (\bar{A}_2 \cdot \bar{p}) \bar{p} \left[ 2\bar{q} \cdot \frac{\bar{p}}{m} \right] \left[ \bar{k} \cdot \frac{\bar{p}}{m} \right] G_-^2 G_+^4, \end{aligned} \quad (4.18)$$

$$\bar{M}_c = (\bar{A}_2 \cdot \bar{p}) \bar{p} G_-(\bar{p} + \bar{q})G_+^2(p)G_+(\bar{p} + \bar{k}) = (\bar{A}_2 \cdot \bar{p}) \bar{p} \left[ \bar{q} \cdot \frac{\bar{p}}{m} \right] \left[ \bar{k} \cdot \frac{\bar{p}}{m} \right] G_-^2 G_+^4. \quad (4.19)$$

The total contribution is

$$\bar{M}_a + \bar{M}_b + \bar{M}_c = (\bar{A}_2 \cdot \bar{p}) \bar{k} \left[ \bar{q} \cdot \frac{\bar{p}}{m} \right] G_-^2 G_+^3 + (\bar{A}_2 \cdot \bar{p}) \bar{p} \left[ \bar{k} \cdot \frac{\bar{p}}{m} \right] \left[ \bar{q} \cdot \frac{\bar{p}}{m} \right] (2G_-^3 G_+^3 + 3G_-^2 G_+^4) = 0. \quad (4.20)$$

The cancellation is shown by a direct evaluation in the way done in Eq. (3.5). Similar considerations show the cancellation of the current vertex  $\bar{M}$  which carries a momentum  $\bar{k}$ .

The conclusion of the above rather involved calculation is that

$$\delta\sigma_H = 0. \quad (4.21)$$

The conclusion is not changed when the Hartree terms are included. In terms of the Hall constant, we have

$$\frac{\delta R_H}{R_H} = 2 \frac{\delta R}{R}. \quad (4.22)$$

This result is to be contrasted with the localization theory Eq. (3.13) and also with the naive single particle picture of the resistivity rise due to a carrier number reduction. In that picture  $R_H = 1/nec$  and  $\delta R_H/R_H = \delta R/R$ .

## V. CONCLUSION

In this paper we studied the effects of a magnetic field on two very different models. Both models predict similar logarithmic rise in resistivity at low temperatures. The first model deals with the localization of noninteracting electrons. We find that the temperature-dependent resistivity is suppressed by very small magnetic fields. Furthermore a strong negative magnetoresistance is predicted. This latter prediction appears to be observed experimentally in the silicon inversion layer.<sup>18</sup> On the other hand no logarithmic correction in the Hall constant is predicted at low temperatures in the localization model. The second model deals with interacting electrons in the presence of weak impurity scattering. Since the divergent resistivity comes from particle-hole diffusion, a static magnetic field is not expected to have strong effects on the divergence. The Hall constant is predicted to increase logarithmically at low tem-

perature, but at a rate equal to twice that of the resistivity. It is hoped this work will help decide which of the two models is more closely related to experiments.

## ACKNOWLEDGMENT

This work is the result of our participation in the Joint Research Group in Condensed Matter Physics of the Joint US-USSR Commission on Scientific and Technological Cooperation that met in Lake Sevan, Armenia, USSR.

## APPENDIX A

In this appendix we compute  $\bar{P}_0$  defined in Eq. (2.5). To do so requires solving the integral equation

$$\int \bar{P}_0(\bar{r}, \bar{r}') \psi_\eta(\bar{r}') d\bar{r}' = \lambda(\eta) \psi_\eta(\bar{r}). \quad (A1)$$

By combining Eqs. (2.5) and (2.6) we obtain

$$\int P_0(\bar{r} - \bar{r}') \exp\left(2ie \int_{\bar{r}}^{\bar{r}'} \bar{A}(\bar{s}) \cdot d\bar{s}\right) \psi_\eta(\bar{r}') d\bar{r}' = \lambda(\eta) \psi_\eta(\bar{r}), \quad (A2)$$

where  $P_0$  is the zero-field propagator with a Fourier transform given by Eq. (2.2). Equation (A2) can be converted to a differential equation of infinite order and solved.<sup>19</sup> For our purpose it suffices to expand  $A(\bar{s})$  and  $\psi_\eta(\bar{r}')$  about  $\bar{r}$  to second order to produce the following differential equation:

$$\left[ P_0(q=0) + \frac{1}{2} \frac{\partial^2 P_0}{\partial q^2} \Big|_{q=0} \left( \frac{\nabla}{i} + 2eA \right)^2 \right] \psi_\eta(\bar{r}) = \lambda(\eta) \psi_\eta(\bar{r}). \quad (A3)$$

This simply shows that to this order, the effect of a magnetic field is represented by  $\nabla/i \rightarrow \nabla/i + 2eA$ . Using Eq. (2.2) we readily see that Eq. (A3) is the

Landau equation for a doubly charged particle in a magnetic field. Equation (2.7) follows immediately.

### APPENDIX B

In this appendix we examine some consequences of using the divergence in the particle-particle channel in the interaction theory. Let us consider the self-energy correction. We have an exchange contribution shown in Fig. 7(a). In Ref. 11 we pointed out that the Hartree diagram 7(b) may also be important if the interaction is short range. In the Hartree term the momentum transfer in the interaction line is not small and must be integrated over. Separating out the integration over  $\vec{p}'$ ,  $\vec{p}''$  in Fig. 7(b), we see that the Hartree term is reduced from the exchange term by a factor

$$F = u^4 \sum_{\vec{p}', \vec{p}''} G_+(\vec{p}') G_-(\vec{p}') \times \frac{v(\vec{p}' - \vec{p}'')}{v(0)} G_+(\vec{p}'') G_-(\vec{p}''). \quad (\text{B1})$$

In the limit  $\tau^{-1} \rightarrow 0$ , the magnitude of  $\vec{p}'$  and  $\vec{p}''$  are near the Fermi wave vector. Only the angular integration remains, where  $\theta$  is the angle between  $\vec{p}'$  and  $\vec{p}''$ . In two dimensions the static screened Coulomb interaction is

$$v(q) = \frac{2\pi e^2}{|\vec{q}| + \kappa}, \quad (\text{B2})$$

where  $\kappa = 2\pi e^2 s N_1$  is the inverse screening length. The momentum transfer  $|\vec{p} - \vec{p}''| = 2k_F \sin\theta/2$ , so

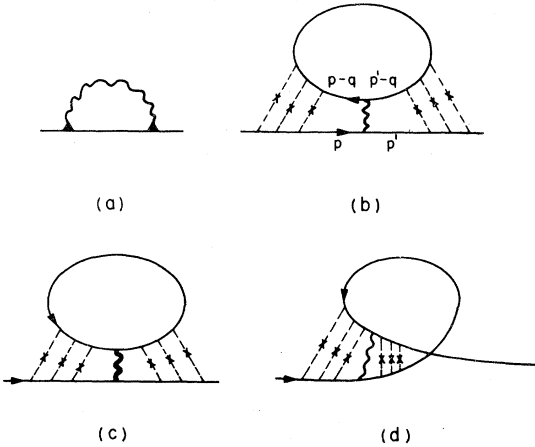


FIG. 7. Self-energy correction from (a) exchange and (b) Hartree diagrams. Figure 7(c) shows the Hartree diagram with the ladder sum in the particle-particle channel and Fig. 7(d) is the exchange counterpart.

that Eq. (B1) becomes

$$F = \int \frac{d\theta}{2\pi} \frac{1}{1 + (2k_F/\kappa) \sin\theta/2}. \quad (\text{B3})$$

Clearly  $F$  approaches unity if  $2k_F/\kappa \rightarrow 0$  and zero for large  $2k_F/\kappa$ .

It is natural to consider next the Hartree term shown in Fig. 7(c) which makes use of the divergence in the particle-particle channel. It equals Fig. 7(b) in the absence of any delocalizing factors, such as spin-flip scattering or magnetic fields. The corresponding exchange term is shown in Fig. 7(d). However it is different from Fig. 7(a) in that the momentum transfer in the interaction line is not small. Clearly Fig. 7(d) is smaller than Fig. 7(a) by the same factor  $F$  given in Eq. (B3).

We thus conclude that if the interaction range is long ( $2\kappa_F/k \rightarrow \infty$ ), the exchange diagram 7(a) dominates over the singularity caused by the particle-particle channel as well as the Hartree term. In the opposite limit of a short-range potential, the Hartree term becomes important as well as the particle-particle channel. However, the latter can be suppressed by spin-flip scattering or a magnetic field.

At this point we also insert a note on the effects of orbital degeneracy in the Hartree term. Such questions may be relevant to the silicon inversion layer. Let us consider a model with two degenerate valleys located at  $\pm K$ . In the absence of intervalley scattering, the Hartree term clearly has an additional factor of 2 from the orbital degeneracy. In practice a short-range impurity potential can produce intervalley scattering. Let us say that the electron is initially in valley  $+K$ . Then the electron loop in Fig. 7(b) can either be in the  $\pm K$  valley but these will have different values. If the closed loop is also  $+K$ , intervalley scattering can take the particle-hole pair to the  $-K$  valley. On the other hand if the loop is  $-K$ , intervalley scattering does not operate because of the conservation of momentum on the average. In the latter case the divergence is cut off if the intervalley scattering rate  $\tau_0^{-1}$  is greater than  $\Omega$  or  $T$ . In this case the orbital dependency does not appear in the Hartree term.

### APPENDIX C

In this appendix we demonstrate the cancellation between the conductivity diagrams [Figs. 5(a), 5(b), and 5(c)]. The diffusion pole plays no role in this cancellation, and we represent it by

$$f(\omega) = \int \frac{d^2q}{(2\pi)^2} \frac{v_s(q, \omega)}{(-i\omega + Dq^2)^2}. \quad (\text{C1})$$

Let us first consider Fig. 5(a). It is necessary to

break up its contribution depending on the sign of  $\epsilon$  and  $\epsilon + \Omega$ . We adopt the notation  $a_{++}$  as the contribution from Fig. 5(a) when  $\epsilon > 0$  and  $\epsilon + \Omega > 0$ , etc. For  $a_{++}$  we note from Eq. (4.4) that in order to get the diffusion pole, we must have  $\epsilon + \omega + \Omega < 0$ .

This gives

$$a_{++} = \int_0^\infty d\epsilon \int_{-1/\tau}^{-\epsilon-\Omega} d\omega f(-\omega) \sum_{\vec{p}} p_F^2 G_+^3(\vec{p}) G_-(\vec{p}) . \quad (C2)$$

Similarly

$$a_{--} = \int_0^\infty d\epsilon \int_{\epsilon-\Omega}^{1/\tau} d\omega f(\omega) \sum_{\vec{p}} p_F^2 G_-^3(\vec{p}) G_+(\vec{p}) . \quad (C3)$$

Integration by parts yield the following equalities:

$$\begin{aligned} P &= \sum_{\vec{p}} p_F^2 G_+^3 G_- = \sum_{\vec{p}} p_F^2 G_+ G_-^3 = -\frac{1}{2} \sum_{\vec{p}} p_F^2 G_+^2 G_-^2 \\ &= -2\pi p_F^2 N_1 \tau^3 . \end{aligned} \quad (C4)$$

In addition to Fig. 5(a) there is the diagram with the self-energy correction on the hole line. We denote its contribution by  $a'_{++}$ , etc. We find that

$$a_{++} = a'_{--} , \quad a_{--} = a'_{++} . \quad (C5)$$

Next we consider Fig. 5(b). The only contributions are  $b_{++}$  and  $b_{--}$  and we find

$$b_{++} = b_{--} = \int_0^\infty d\epsilon \int_{\epsilon}^{1/\tau} d\omega f(\omega) \sum_{\vec{p}} p_F^2 G_+^2 G_-^2 . \quad (C6)$$

Combining Eq. (C1) to Eq. (C5) we have

$$\begin{aligned} a_{++} + a_{--} + a'_{++} + a'_{--} + b_{++} + b_{--} \\ = 2P \int_0^\infty d\epsilon \int_{\epsilon}^{1/\tau} d\omega f(\omega) . \end{aligned} \quad (C7)$$

$$\begin{aligned} a_{3--} &= \sum_p \vec{A}_1 \cdot (\vec{p} - \vec{k}) (\vec{p} \cdot \vec{A}_2) \left[ \vec{p} - \frac{\vec{k}}{2} \right] G_-^2(\vec{p} - \vec{k}) G_-^2(\vec{p}) G_+(\vec{p}) \\ &= - \sum_{\vec{p}} (\vec{A}_1 \cdot \vec{k}) (\vec{p} \cdot \vec{A}_2) \vec{p} G_-^4 G_+ - \sum_{\vec{p}} (\vec{A}_1 \cdot \vec{p}) (\vec{A}_2 \cdot \vec{p}) \left[ \vec{k} \cdot \frac{\vec{p}}{m} \right] \vec{p} (2G_-^2 G_+) , \end{aligned} \quad (D1)$$

$$a_{4--} = \sum_p (\vec{A}_1 \cdot \vec{p}) (\vec{A}_2 \cdot \vec{p}) \left[ \vec{k} \cdot \frac{\vec{p}}{m} \right] \vec{p} (G_-^3 G_+^3 + G_+^2 G_-^4) , \quad (D2)$$

where we have kept only terms that will produce  $(\vec{A}_1 \cdot \vec{k}) \vec{A}_2$  as discussed in Sec. III. Next we consider the diagrams with the self-energy on the hole line. According to Eq. (C5) the diagrams with the same limits of integration are those with  $\epsilon > 0$  and  $\epsilon + \Omega > 0$ . Denoting these by  $a'_{3++}$  and  $a'_{4++}$  we find

Next we consider Fig. 5(a) with  $\epsilon < 0$  and  $\epsilon + \Omega > 0$ .

$$\begin{aligned} a_{-+} + a'_{-+} &= 2 \int_{-\Omega}^0 d\epsilon \int_{\epsilon+\Omega}^{1/\tau} d\omega f(\omega) \sum_{\vec{p}} p_F^2 G_+^2 G_-^2 \\ &= -4P \int_0^\Omega d\epsilon \int_{\epsilon}^{1/\tau} d\omega f(\omega) . \end{aligned} \quad (C8)$$

Finally we have Fig. 5(c) which is a correction to the scattering rate due to the density of state correction

$$\begin{aligned} \delta\tau^{-1} &= u^2 \int_{\epsilon}^{1/\tau} d\omega f(\omega) \sum_{\vec{p}} G_+^2(\vec{p}') G_-(\vec{p}') \\ &= -i\tau \int_{\epsilon}^{1/\tau} d\omega f(\omega) , \end{aligned} \quad (C9)$$

where we have used  $\tau^{-1} = 2\pi N_1 u^2$ . In Fig. 5(c) only the case  $\epsilon < 0$ ,  $\epsilon + \Omega > 0$  contributes, giving

$$\begin{aligned} c_{-+} + c'_{-+} &= 2 \int_0^\Omega d\epsilon \delta\tau^{-1}(\epsilon) \sum_{\vec{p}} p_F^2 G_+^2 G_- \\ &= -4\pi N_1 \tau^3 p_F^2 \int_0^\infty d\epsilon \int_{\epsilon}^{1/\tau} d\omega f(\omega) . \end{aligned} \quad (C10)$$

Combining Eqs. (C7), (C8), (C10), and (C4) we see that all the diagrams sum to zero.

## APPENDIX D

In this appendix we show that the Hall diagrams generated from the conductivity diagrams considered in Appendix C also cancel.

First we note that diagrams generated from Fig. 5(b) occur in pairs [Figs. 8(b<sub>1</sub>) and 8(b<sub>2</sub>)] so that their sum is even in  $\vec{k}$  and therefore vanishes. Figures 8(a<sub>1</sub>) to 8(a<sub>4</sub>) are the diagrams generated from Fig. 5(a). First we consider the case  $\epsilon < 0$ ,  $\epsilon + \Omega < 0$ . Then  $a_{1--} + a_{2--}$  is also even in  $k$ . We are left with

that  $a'_{3++} = -a_{3--}^*$  and  $a'_{4++} = -a_{3--}^*$ , so that

$$X_1 = a_{3--} + a_{4--} + a'_{3++} + a'_{4++} \quad (D3)$$

is purely imaginary.

These diagrams are now to be combined with  $X_2 = a_{3++} + a_{4++} + a'_{3--} + a'_{4--}$ . As seen from Eqs.

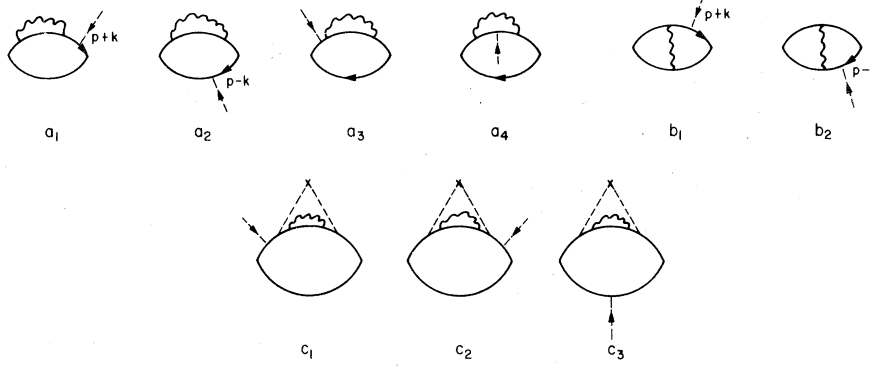


FIG. 8. Hall Effect diagrams generated by adding magnetic vertex (dashed line) carrying momentum  $k$  into Figs. 5(a), 5(b), and 5(c).

(C2) and (C3),  $X_1$  and  $X_2$  have different limits of integration. Furthermore the integrands of  $X_1$  and  $X_2$  are complex conjugates of each other. Since  $X_1$  is purely imaginary, we find

$$X_1 + X_2 = \int_0^\Omega d\epsilon \int_\epsilon^{1/\tau} d\omega f(\omega) \sum_{\vec{p}} \left\{ \left[ -(\vec{A}_1 \cdot \vec{k})(\vec{p} \cdot \vec{A}_2) \vec{p} G_\pm G_\pm + (\vec{A}_1 \cdot \vec{p})(\vec{p} \cdot \vec{A}_2) \left( \vec{k} \cdot \frac{\vec{p}}{m} \right) \vec{p} (G_\pm^2 G_\pm - 2G_\pm G_\pm) \right] - \text{c.c.} \right\}. \quad (\text{D4})$$

Next we perform similar calculation for

$$Y = a_{1-+} + a_{2-+} + a_{3-+} + a_{4-+} + a'_{1-+} + a'_{2-+} + a'_{3-+} + a'_{4-+}. \quad (\text{D5})$$

Again  $a'_{1-+} = -a_{1-+}^*$ , etc., and we find

$$Y = \int_0^\Omega d\epsilon \int_\epsilon^{1/\tau} d\omega f(\omega) \sum_{\vec{p}} (\vec{k} \cdot \vec{A}_1)(\vec{p} \cdot \vec{A}_2) \vec{p} \times (G_\pm^2 G_\pm - \text{c.c.}). \quad (\text{D6})$$

Using the following identities

$$\sum_{\vec{p}} \left( \frac{p^2}{2m} \right)^2 (G_\pm^2 G_\pm - \text{c.c.}) = -8\pi i \epsilon_F \tau^4 N_1, \quad (\text{D7})$$

$$\sum_{\vec{p}} \left( \frac{p^2}{2m} \right)^2 (G_+ G_- - \text{c.c.}) = 4\pi i \epsilon_F \tau^4 N_1, \quad (\text{D8})$$

$$\sum_{\vec{p}} G_\pm^2 G_\pm = 6\pi i \tau^4 N_1, \quad (\text{D9})$$

we obtain

$$X_1 + X_2 + Y = \int_0^\Omega d\epsilon \int_\epsilon^{1/\tau} d\omega f(\omega) (\vec{A}_1 \cdot \vec{k}) \vec{A}_2 \epsilon_F 8\pi i \tau^4. \quad (\text{D10})$$

Finally we are left with diagrams generated from Fig. 5(c). It can be shown that insertions of the magnetic vertex inside the impurity-scattering self-energy part are canceled, so that we are left with  $c_1, c_2$ , and  $c_3$  and the corresponding  $c'_1 + c'_2 + c'_3$  which equals  $c_1 + c_2 + c_3$ . The total contribution is

$$2(c_{1-+} + c_{2-+} + c_{3-+}) = 2 \int_0^\Omega d\epsilon \int_\epsilon^{1/\tau} d\omega f(\omega) (\delta\tau^{-1}) \sum_{\vec{p}} (\vec{A}_1 \cdot \vec{p})(\vec{A}_2 \cdot \vec{p}) \left( \vec{k} \cdot \frac{\vec{p}}{m} \right) \vec{p} (3G_- G_+^2 - G_+^2 G_-^2). \quad (\text{D11})$$

Using Eq. (C9) and upon evaluation of the integrals we find that Eq. (D11) exactly cancels  $X_1 + X_2 + Y$  given by Eq. (D10).

- <sup>1</sup>E. Abrahams, P. W. Anderson, D. C. Licciardello, and T. V. Ramakrishnan, *Phys. Rev. Lett.* **42**, 673 (1979); E. Abrahams and T. V. Ramakrishnan, *J. Non-Cryst. Solids* **35**, 15 (1980).
- <sup>2</sup>F. Wegner, *Z. Phys. B* **35**, 207 (1979).
- <sup>3</sup>L. P. Gor'kov, D. Khmel'nitzkii, and A. I. Larkin, *Pisma Zh. Eksp. Teor. Fiz.* **30**, 248 (1979).
- <sup>4</sup>D. Khmel'nitzkii (unpublished).
- <sup>5</sup>W. Götze, *Solid State Commun.* **27**, 1393 (1978); W. Götze, P. Prelovsek, and P. Wölfe, *Solid State Commun.* **30**, 369 (1979).
- <sup>6</sup>P. A. Lee, *Phys. Rev. Lett.* **42**, 1492 (1979).
- <sup>7</sup>P. A. Lee, *J. Non-Cryst. Solids* **35**, 21 (1980).
- <sup>8</sup>S. Hikami, A. I. Larkin, and Y. Nagaoka, *Prog. Theor. Phys.* **63**, 707 (1980).
- <sup>9</sup>G. J. Dolan and D. D. Osheroff, *Phys. Rev. Lett.* **43**, 721 (1979).
- <sup>10</sup>D. J. Bishop, D. C. Tsui, and R. C. Dynes, *Phys. Rev. Lett.* **44**, 1153 (1980).
- <sup>11</sup>B. L. Altshuler, A. G. Aronov, and P. A. Lee, *Phys. Rev. Lett.* **44**, 1288 (1980).
- <sup>12</sup>B. L. Altshuler and A. G. Aronov, *Solid State Commun.* **36**, 115 (1979).
- <sup>13</sup>See, for example, L. P. Gor'kov, *Zh. Eksp. Teor. Fiz.* **36**, 1918 (1959) [*Sov. Phys. JETP* **36**, 1364 (1959)].
- <sup>14</sup>D. J. Thouless, *Phys. Rev. Lett.* **39**, 1167 (1977).
- <sup>15</sup>P. W. Anderson, E. Abrahams, and T. V. Ramakrishnan, *Phys. Rev. Lett.* **43**, 718 (1979).
- <sup>16</sup>H. Fukuyama *J. Phys. Soc. Jpn.* **49**, 644 (1980).
- <sup>17</sup>N. Giordano, W. Gilson, and D. E. Prober, *Phys. Rev. Lett.* **43**, 725 (1979).
- <sup>18</sup>Y. Kawaguchi and S. Kawaji, *J. Phys. Soc. Jpn.* **48**, 699 (1980).
- <sup>19</sup>P. A. Lee and M. G. Payne, *Phys. Rev. B* **5**, 923 (1972).